Different state-dependence of population codes across cortex

Akhil C. Bandi[1,3], Caroline A. Runyan[2,3]

[1]Neuroscience Institute, Carnegie Mellon University, Pittsburgh, PA

[2]Department of Neuroscience, University of Pittsburgh, Pittsburgh, PA

[3]Center for the Neural Basis of Cognition, University of Pittsburgh, Pittsburgh, PA

Summary

During perceptual decision-making, behavioral performance varies with changes in internal states such as arousal, motivation, and strategy. Yet it is unknown how these internal states affect information coding across cortical regions involved in differing aspects of sensory perception and decision-making. We recorded neural activity from the primary auditory cortex (AC) and posterior parietal cortex (PPC) in mice performing a navigation-based sound localization task. We then modeled transitions in the behavioral strategies mice used during task performance. Mice transitioned between three latent performance states with differing decision-making strategies: an 'optimal' state and two 'sub-optimal' states characterized by choice bias and frequent errors. Performance states strongly influenced population activity patterns in association but not sensory cortex. Surprisingly, activity of individual PPC neurons was better explained by external inputs and behavioral variables during suboptimal behavioral performance than in the optimal performance state. Furthermore, shared variability across neurons (coupling) in PPC was strongest in the optimal state. In AC, shared variability was similarly weak across all performance states. Together, these findings indicate that neural activity in association cortex is more strongly linked to internal state than in sensory cortex.

Introduction

As an animal makes decisions based on relevant sensory information, its behavior can shift between periods of optimal and suboptimal performance. These fluctuations in performance are guided by changes in the internal state of the animal, such as its level of arousal or motivation (Flavell et al., 2022; Livneh & Andermann, 2021). These fluctuations in task performance can be

modeled as discrete decision-making strategies guiding choice behavior (Ashwood et al., 2022; Bolkan, Stone et al., 2022). Animals trained to expertly perform decision-making tasks predominantly occupy an optimal performance state, as evidenced by high task accuracy and enhanced attention to sensory information (Harris & Thiele, 2011). When animals occupy suboptimal performance states, although they are still engaged in decision-making behavior, they experience increased lapses in choices, and increased variability on correlates of arousal such as pupil diameter and uninstructed movements (Hulsey et al., 2024).

Task-relevant information, such as sensory stimuli and behavioral choices, is encoded across sensory and association-level cortex (Runyan et al., 2017; Steinmetz et al., 2019; Tseng et al., 2022). The primary auditory cortex (AC) processes incoming sound information but is also modulated by task performance (Fritz et al., 2003; Heller et al., 2023; Kuchibhotla et al., 2017), arousal state (Khoury et al., 2023; Lin et al., 2019; McGinley et al., 2015), and motor behavior (Nelson & Mooney, 2016; Schneider et al., 2014, 2018). Downstream association-level cortices, such as posterior parietal cortex (PPC), integrate sound information with other relevant information to guide perceptual decisions. Both AC and PPC are characterized by rich population activity dynamics (Aponte et al., 2021; Aschauer et al., 2022; Downer et al., 2021; Driscoll et al., 2017; Mohan et al., 2021), and in both regions, shared variability in the activity across neurons is modulated by task performance and arousal level (Khoury et al., 2023; McGinley et al., 2015). However, shared variability is overall stronger and has a longer timescale in PPC (Runyan et al., 2017). Both AC and PPC are diversely connected with other brain regions such as other association cortices and subcortical structures (Lyamzin & Benucci, 2019), and contribute to perceptual decision-making (Akrami et al., 2018; Guo et al., 2017; Pho et al., 2018; Song et al., 2017; Zhong et al., 2019).

Although task engagement impacts sensory responses in AC and PPC, it is unclear how transitions in the internal states that naturally occur within the task performance context impact information coding across these two different levels of cortical processing. Do suboptimal

performance states hinder representations of task information in both AC and PPC, or is one region more impacted by state than the other? Furthermore, do optimal performance states affect the shared variability of activity between neurons, an important feature of population activity, and is this effect consistent across the cortical hierarchy?

To answer these questions, we identified latent states that explained variations in mouse performance of an auditory decision-making task, including a near-optimal performance state and heavily biased, suboptimal performance states. We then related these states to neural population coding for task-related information in AC and PPC. Coding was differently impacted in the two areas across performance states. In AC, population activity patterns were highly similar across states. In contrast, population activity patterns differed significantly across performance states in PPC in three key ways: 1) PPC activity could be used to identify the latent behavioral state, 2) stimulus decoding using PPC activity was enhanced in high performance states, and 3) shared variability across neurons was greater in PPC during the optimal performance state. Our results reveal that latent performance states during decision-making have a diverse range of effects on information coding in the activity of different cortical regions, and optimal performance states drive association but not sensory cortex into correlated and functionally coupled regimes.

Results

Mice switch between performance states during auditory decision-making

Mice performed a two-armed forced choice, virtual reality (VR) based T-maze task, using the locations of sound stimuli to guide left-right choices (n=5, Runyan et al., 2017). As mice ran down a T-stem of the virtual reality corridor a sound cue was played from one of eight possible locations. Mice reported whether the sound came from a left or right direction by turning in that direction at the T-intersection (Figure 1A). Expert mice learned to accurately categorize the locations of the sound cues, making greater than 70% correct choices in a session, and used a subjective category boundary (as shown by the peak of the psychometric slope function) that closely matched the experimentally defined category boundary (Figure 1B). However, even expert

mice fluctuated in task performance within single behavioral sessions (Figure 1C-top), and periods of low task performance were found to have an increased choice bias regardless of the sound localization cue (Figure 1C-middle, bottom).

To characterize these fluctuations in task performance and identify potential changes in hidden states guiding behavioral performance, we used hidden Markov models with generalized linear model observations (GLM-HMMs, Ashwood et al., 2022). We modeled the mouse's decision-making strategy using a GLM-HMM with four inputs (Figure 1D): (1) the left-right location category of the auditory stimulus on the present trial; (2) the binary (left-right) choice made by the mouse on the previous trial; (3) whether the previous trial was correct or incorrect; (4) and a constant offset or choice bias. Thus, each 'state' in the HMM corresponds to a Bernoulli GLM for a rightward choice given the four input predictors. We fit GLM-HMMs with varying numbers of latent states to choice data from 69 total behavioral sessions across 5 mice performing the VR sound localization task and found that a three-state GLM-HMM explained the data well, as evidenced by high log-likelihood and predictive accuracy on held-out test data (Extended figure 1).

Examining the inferred GLM weights related to the mouse's choice in each state revealed that the state 1 GLM had a large weight for sound stimulus location and negligible weights for previous choice, previous reward outcome, and choice bias. The GLMs for state 2 and state 3, had small weights for stimulus location and high and opposing weights for the left-right bias input (Figure 1E). State 1 was the most frequently occupied state across all behavioral sessions (53.5±11.8%), and when mice occupied this state their task performance was high (88.0±1.2% correct). States 2 and 3 were less frequently occupied (23.7±12.4% and 22.7±1.8%), and mice during these states had low task performance (58±6.2% and 56±2.2% correct), however they still performed higher than chance (Figure 1F-G). We assessed the decision-making strategies associated with each state by plotting psychometrics curves for the probability of a rightward choice as a function of the stimulus location (Figure 1H). The state 1 psychometric had a steep

slope indicating that the mouse more optimally categorized both easy and difficult sound locations. By comparison, the psychometric curves for state 2 and state 3 had shallow slopes and were shifted up or down, reflecting rightward and leftward choice biases, respectively.

To characterize the temporal structure of how mice transitioned between states during performance of the task, we used the three state GLM-HMM to compute the posterior probability over the mouse's latent state across all trials (Figure 1I). States persisted for many trials in a row (state 1: 20.2±8.2 trials, state 2: 8.6±2.0 trials, state 3: 6.9±1.3 trials), and multiple state transitions occurred throughout a behavioral session (11.3±6.9 state switches). The model had high confidence of the mouse's assigned state during behavior, predicting the most probable state with a probability greater than 0.9 on 87% of trials. Overall, the three-state GLM-HMM revealed that mice trained to expertly perform a VR sound localization task transitioned between optimal and suboptimal latent states of behavioral performance, characterized by unique strategies governing behavioral choices.

Performance states differently impact information coding in sensory and association cortex population activity

To elucidate the effects of behavioral performance state on cortical representations of task-relevant information across different cortical regions, we related occupancy in the 3 GLM-HMM states to patterns of neural activity in AC and PPC. We used in-vivo calcium imaging to monitor the activity of GCaMP6^{+} neurons in AC and PPC on separate days (Figure 2A; N = 203 PPC neurons from 5 behavioral sessions and 178 AC neurons from 4 behavioral sessions). First, we tested if population activity patterns of AC and PPC neurons distinguished between the mouse performing the task in an optimal (state 1) or suboptimal performance state (states 2 or 3). We trained binary support vector machine (SVM) decoders to classify each trial as state 1 or not state 1 (combining states 2 and 3) from AC or PPC neuronal population activity during that trial and calculated the decoding accuracy using five-fold cross validation (Figure 2B). The accuracy of PPC population decoding of performance state was significantly higher than chance ($p= 5.9 \times 10^{-}$

^{7}, Wilcoxon signed rank test), in stark comparison to AC population decoding of performance state which was not significantly different from chance performance (p= 0.67, Wilcoxon signed rank test). This result shows that performance state, as identified by the GLM-HMM, could be discriminated by population activity in PPC but not AC.

Next, we tested if behavioral performance state affected population coding for stimulus and choice variables. We trained SVM decoders to classify left or right stimulus trials from AC or PPC population activity, which was aligned to the onset of the first sound in the trial. One decoder was trained on population activity and trial information from exclusively state 1 trials ('state 1 decoder') and another was trained on population activity and trial information from trials spanning all performance states ('all-state decoder'). The all-state decoder included data from state 2 and state 3 trials supplemented with subsampled state-1 trials to ensure similar numbers of trials for comparisons between the two types of decoders (Extended Figure 3A). The accuracy of stimulus classification from AC population activity peaked at one second post sound onset for both decoders and both had similar peak decoding accuracy (Figure 2C). Conversely, the accuracy of stimulus classification from PPC population activity over time was different between the two decoders: state 1 decoder had consistently higher stimulus classification accuracy than the all-state decoder (Figure 2D).

We repeated this SVM decoding approach for classification of left or right choice trials from AC or PPC neuronal population activity but aligned activity instead to the onset of the turn into the left or right arm of the VR maze. The accuracy of choice classification from AC population activity was similarly low in the state 1 and all-state decoders (Figure 2E), while the accuracy of choice classification from PPC population activity was different across the two decoders (Figure 2F). Both decoders trained to classify choice from PPC population activity had peak classification accuracy at the time of turn onset, and classification accuracy was higher for the state-1 decoder in comparison to the all-state decoder. Together, these results indicate that task-relevant

information in association cortex but not sensory cortex population activity patterns were modulated by the performance state of the animal.

Behavioral variables better predict PPC activity during suboptimal performance states

Neural activity in AC and PPC is heterogeneous, affected by stimulus, choice, and various other task-relevant variables such as reward delivery, the mouse's position in the maze, and its running patterns (Goard et al., 2018.; Harvey et al., 2012; Minderer et al., 2019; Runyan et al., 2017). To understand the relationship between these diverse variables and the neuronal responses in AC and PPC, we followed an encoding model approach using generalized linear models (GLMs, (Runyan et al., 2017)). The GLMs, which used all measured task-relevant variables as predictors of each AC or PPC neuron's activity, were trained and tested using trials that occurred during different behavioral performance states, as defined by the GLM-HMM above. The first set of models included only performance state 1 ('state 1 encoding model'), and the second set of models were trained and tested using trials from all three performance states ('all-state encoding model').

To compare encoding properties across behavioral performance states in each AC or PPC neuron, we compared the state 1 encoding model's prediction performance (measured as the fraction of explained deviance in held-out trials) to the all-state encoding model's prediction performance. We could then use this comparison to estimate the impact of suboptimal performance states on encoding of information in neuronal activity. In AC, the prediction performance of the two encoding models was similar (n=171 AC neurons, p=.18, Mann-Whitney U-test, Figure 3B). Surprisingly, the activity of most PPC neurons was better predicted by the all-state encoding model (n=203 PPC neurons, $p=1.8 \times 10^{-5}$, Mann-Whitney U-test, Figure 3C). This suggests that task-relevant variables were equal predictors of neuronal activity in AC across performance states but were stronger predictors of neuronal activity in PPC when mice occupied the suboptimal performance state.

To understand these seemingly paradoxical results, that in PPC stimulus and choice decoding were modestly *improved* in the optimal state (Figure 2) but that the encoding model prediction performance was *worse* in optimal behavioral state (Figure 3C), we examined the contributions of different categories of predictors in explaining neurons' activity across states in the encoding model. To assess to total weighting of each category of predictor, we summed the coefficients for each type of predictor (e.g. sound stimuli) from the model fits for each AC and PPC neuron. Sound stimulus predictors were weighted heavily and equally by both sets of encoding models for AC neurons. In contrast, for PPC neurons there was a significant difference in the magnitude of the sound stimulus predictor coefficients between the two encoding models. Sound predictors had large coefficients only in the all-state encoding model but not the state-1 encoding model (Figure 3D). A similar trend persisted for position/choice predictors and running velocity predictors (Figure 3E-F). Collectively, the results from this encoding model analysis show that the activity of sensory cortex neurons is similarly explained by stimulus and behavioral variables regardless of performance state, while the activity of association cortex neurons is more strongly explained by these variables when mice are in suboptimal states.

Functional coupling between neurons increased in PPC during optimal performance states

When mice performed the task more optimally (occupying state 1), the decoding of task information (i.e. stimulus and choice) from PPC population activity was slightly higher, but, surprisingly, task and behavioral information more poorly predicted PPC neuronal activity. This mismatch indicated that our encoding models, built solely on task information, were missing other relevant predictors of PPC neuronal activity, especially during optimal performance states. Previous work has shown that functional coupling, or shared variability among neurons in local populations, is higher in association than sensory cortex, and affects information coding and behavioral accuracy (Valente et al., 2021). We first asked whether functional interactions among neurons in AC and PPC varied across performance states, by computing pairwise noise correlations, the Pearson correlation between two neurons' trial-to-trial response variability

(Figure 4A). Noise correlations during the sound onset period in the AC population were similar between optimal and suboptimal performance states (p=.096, Mann-Whitney U-test) but were significantly higher during the optimal performance state in PPC ($p=2.4 \times 10^{-9}$, Mann-Whitney U-test) during the turn onset period. This indicated that functional coupling in the PPC population was more pronounced during periods of optimal task performance and could therefore be a key predictor of neuronal activity.

To test this hypothesis and measure functional coupling in PPC population activity across performance states, we modified our encoding models to predict a given neuron's activity based on task information and the activity of the other neurons in the population (Figure 4B). We extracted the first five principal components (PCs), identified via principal component analysis, of the population response (excluding the activity of the predicted neuron) and convolved these PCs with gaussian basis functions to model correlations across time (Runyan et al., 2017). We refit both the all-state and state-1 encoding models for each AC or PPC neuron with these ten additional 'functional coupling' predictors and compared prediction performance with and without population activity to measure the contribution of functional coupling to each neuron's activity. For the all-state encoding model, adding functional coupling predictors had no significant effect on prediction performance of neuronal activity in both AC and PPC (Figure 4D, AC: p=.106, PPC: p=.588, Mann-Whitney U-test). This was also true for the state 1 encoding model fit to AC neuronal activity. However, adding functional coupling predictors to the state 1 encoding model for PPC neurons significantly increased prediction performance (Figure 4C, AC: p=.438, PPC: $p=6.2 \times 10^{-5}$, Mann-Whitney U-test)) in comparison to the state 1 model without population activity. Additionally, an examination of the model weights for the functional coupling predictors for each model revealed that coupling weights were larger in the state-1 model than in the all-state model, only for PPC neurons (Figure 4E). Together, these findings reveal that when mice exclusively occupy an optimal performance state, association cortex but not sensory cortex population

dynamics become functionally coupled and increase relevant information coding in neuronal activity.

Discussion

In this study, we show that internal states related to behavioral performance affect information coding differently in sensory and association cortex. We trained mice to perform an auditory decision-making task, imaged neuronal spike-related activity in AC and PPC and used GLM-HMM modeling to identify distinct states of optimal and suboptimal behavioral performance each with unique decision-making strategies. Similar to the performance states identified during visual decision-making (Ashwood et al., 2022; Bolkan et al., 2022; Hulsey et al., 2024), we identified one optimal state, characterized by high task performance, and two suboptimal states in which mice were biased in their choice behavior toward either left or right choices (Figure 1E-G). Interestingly, though psychometrics in the suboptimal states were poor, we did find conservation of psychometric slope, indicating that animals were still engaged in the task despite adopting a suboptimal strategy.

We used decoding and encoding analyses to relate population activity patterns in AC and PPC to the behavioral performance state of the mouse. One challenge to this approach is that mouse behavior in biased states is, by definition, biased toward one choice direction in a particular state. As a consequence, in an area like PPC where neurons strongly encode choice direction, direct comparison of the three states could lead to trivial conclusions based on the differential choice outcomes in the left and right biased states. It was therefore crucial to balance all possible combinations of stimulus and choice directions to decouple these variables and balance their weighting in the training datasets. We accomplished this by combining the two suboptimal performance states, balancing their trial numbers, in the training and testing datasets for our models. Furthermore, because the mice were trained to become experts at the auditory decision-making task, they tended to predominantly perform the task in the optimal state. The resulting imbalance, in the number of trials performed across the three states, left too few trials to directly

compare population coding between suboptimal and optimal performance states, as these analyses require large numbers of trials to train encoding models and test their prediction performance. We therefore compared population coding in optimal vs 'all' states, combining the two biased states and supplementing with trials during optimal performance.

By training a linear classifier to decode task trials during optimal vs suboptimal states, we discovered that the mouse's behavioral performance state could be decoded from PPC but not AC population activity (Figure 2B). This implies that population activity patterns differed with performance state in PPC, but not AC. Indeed, PPC population activity differed in several key aspects across states. First, the stimuli and behavioral choices in the task could be more accurately decoded using PPC activity during the optimal performance state. Second, task- and movement-related variables better explained PPC activity in the 'all-state' models than in the optimal models. This result was initially surprising but fits well with other findings that uninstructed movements are inversely correlated with behavioral performance and can modulate cortical activity (Musall et al., 2019; Yin et al., 2023). Third, functional coupling among PPC neurons was stronger in the optimal behavioral performance state, consistent with similar comparisons in correct and error trials in the same dataset (Runyan et al., 2017; Valente et al., 2021). This stronger coupling could enable PPC to drive behavioral outputs more strongly in the optimal performance state.

In contrast, shifts in behavioral state had little impact on population activity in AC in our study. We had expected that these shifts in behavioral performance could be related to shifts in the arousal state of the animal. A rich literature has established relationships between arousal state and stimulus coding, firing rates, and shared variability in auditory cortex (Bigelow et al., 2019; Khoury et al., 2023; Lin et al., 2019; McGinley et al., 2015) , and so the current results may seem contradictory. A few possibilities could explain the inconsistency. We did not monitor the pupil diameter of these mice, and so unfortunately, we do not know whether arousal states shifted systematically between the optimal and suboptimal states. However, the psychometric curves

285 measured using suboptimal state trials suggest that although the mice are biased in reporting
286 their choices, they are still engaged in performing the task. Additionally, our mice must be
287 'aroused' to even perform trials in our task design, as they must voluntarily progress through the
288 T-maze by running on the spherical treadmill. We suspect that our mice are always in a relatively
289 aroused state, and so the differences in arousal across GLM-HMM states 1-3 may not be wide
290 enough to differently drive AC activity patterns.

291 **Limitations of the study**

292 In this study, we measured various behavioral features during task performance such as
293 running velocity, sensory stimulus identity and timing, behavioral choice, and reward delivery. We
294 used these variables in our GLM-HMM modeling and GLM encoding analyses, and inferred latent
295 states related to behavior, which we connected to neural activity patterns. These are observational
296 analyses, as we did not experimentally manipulate the animal's behavioral state, but instead
297 compared neural activity across natural fluctuations in performance. Furthermore, neuronal data
298 from AC and PPC was not collected simultaneously, and neurons in either population were not
299 tracked over days. We take this into account when comparing across both regions and recognize
300 that correlations between the two populations could also be modulated by transitions in behavioral
301 state.

302 **Acknowledgements**

303 We thank Chengcheng Huang, and members of the Runyan lab for comments on the
304 manuscript. We thank Christopher Harvey (Harvard Medical School) in whose laboratory the data
305 was collected. We thank the GENIE project (Janelia) for making GCaMP sensors available for
306 use. This work was supported by the NIH Predoctoral Training Grant in Basic Neuroscience
307 T32NS126122-02, Pew Biomedical Scholars Program, the Searle Scholars Program, the
308 Klingenstein-Simons Fellowship Award in Neuroscience, and NIH grants NIMH DP2MH122404
309 and NINDS R01NS121913.

310 **Author Contributions**

A.C.B. and C.A.R. designed the experiments, C.A.R. performed the experiments, A.C.B. performed analyses, and A.C.B. and C.A.R. wrote the paper.

Declaration of Interests

The authors declare no competing interests.

Data and code availability

Analysis code is deposited and publicly available at: https://github.com/acbandi213/Bandi--Runyan-2024.git

Experimental model details

Behavioral and imaging data were collected from five male C57BL/6J mice (The Jackson Laboratory) that were ~ 7 weeks old at the initiation of behavior task training.

Method details

In this study, we performed an independent analysis of publicly available mouse behavioral and calcium imaging experiments described previously (Runyan et al., 2017). A brief summary of the experimental procedures is provided here, and full detailed procedures can be found in the previously published work. All experimental procedures were approved by the Harvard Medical School Institutional Animal Care and Use Committee.

Sound localization task:

Head-restrained mice ran on a spherical treadmill to control movement through a virtual reality T-maze, which was projected on a screen in front of the mouse. The virtual T-maze was constructed using the Virtual Reality Mouse Engine (ViRMEn, Aronov & Tank, 2014) in MATLAB (v2011a). As mice ran down the stem of the T-maze, sound stimuli were 1-2 s dynamic ripples, delivered from one of eight possible locations (−90°, −60°, −30°, −15°, +15°, +30°, +60° and +90°), using speakers centered around the mouse's head. The stimuli began 10cm into the maze and repeated after a 100-ms gap until the mouse reached the T-maze intersection. Mice were required to report the left-right category of the stimulus location by turning in that direction into either the left or right arm at the T-maze intersection. Correct decisions resulted in delivery of a 4 μl sugar water and a 'reward tone', while incorrect decisions resulted in a 'no-reward tone'. Following a correct choice, there was a 3 s inter-trial interval (ITI), and following an incorrect choice there was a 5 s ITI.

In vivo calcium imaging:

363 Imaging was performed on alternating days from the AC and PPC on the left hemisphere
364 of the animal (PPC centered at 2 mm posterior and 1.75 mm lateral to bregma; AC centered at
365 3.0 mm posterior and 4.3 mm lateral to bregma). In each session, ~50 neurons (range, 37–69)
366 were simultaneously imaged using a two-photon microscope (Sutter MOM) operating at a 15.6-
367 Hz frame rate and at a resolution of 256 × 64 pixels (~250 μm × 100 μm). ScanImage (version 3,
368 Vidrio Technologies) was used to control the microscope. Imaging data were acquired at depths
369 of between 150 and 300 μm, corresponding to layers 2/3. Four AC and six PPC fields of view from
370 five mice were analyzed.

371 **Quantification and statistical analysis**

372 *GLM-HMM modeling of behavioral performance:*

373 To quantify transitions between discrete decision-making states within a single behavioral
374 session, we used a hidden Markov model with Bernoulli Generalized Linear Model observations
375 (GLM-HMM) based on a modified version of the SSM python package. The model is defined by
376 a transition matrix containing a fixed set of transition probabilities: $z \in \{1,\ldots,K\}$, and a vector of
377 GLM weights for each state. Each GLM has a unique set of weights w_k that maps external
378 covariates to the probability of choice for each of the *k* states. We coded the external covariates
379 on each trial as follows: (1) the signed location of the auditory stimulus on the present trial; (2) the
380 binary choice (1 for right or 0 for left) made by the mouse on the previous trial; (3) whether the
381 previous trial was correct or incorrect (1 or 0); (4) and a constant offset or bias. The output for
382 each trial was a value of 1 or 0 depending on whether the mouse turned right or left.

383 We first fit the GLM-HMM to all behavioral data using the expectation-maximization (EM)
384 algorithm, again using the SSM python package. The GLM-HMM state was inferred using the
385 posterior probabilities calculated from the preceding trials and the state transition matrix. To select
386 the number of latent states in the model (K) we performed cross-validation of the behavioral data,
387 which revealed that three states allowed the model to plateau in likelihood, calculated via
388 maximum likelihood estimation (MLE). We also measured choice prediction accuracy for the three

389 state GLM-HMM by using the weights of the inferred state to predict the choice on that trial, which
390 is compared to the empirical data thus determining model prediction accuracy. Following this
391 optimization of states, we then fit a single three state GLM-HMM to the observations and inputs
392 concatenating all sessions from a single subject, and again inferred the state occupation
393 estimates using the posterior probabilities calculated from the preceding trials and the state
394 transition matrix. We found that the three states were consistent across all the subjects used in
395 this study and each three state GLM-HMM fit to each individual animal had high log-likelihood
396 and predictive accuracy on held-out test data. For all further analyses, we set an 80% state
397 probability criterion for inclusion of a trial with a performance state, and discounted trials that did
398 not meet the criterion.

399 *SVM decoding of state, stimulus, and choice information:*

400 For population decoding of performance state information, we used a SVM decoder with
401 a linear kernel (C=100, gamma=0.1, identified via best estimate grid search) based on the
402 sklearn.svm python package. Equal numbers of state 1 trials and non-state 1 trials (combining
403 state 2 and 3) were selected, and then balanced to have a structured distribution of trials from
404 each stimulus and choice combination (left stimulus left choice, right stimulus right choice, left
405 stimulus right choice, right stimulus left choice). We trained the SVM decoder to classify a trial as
406 state-1 or not state-1 (combining states 2 and 3) from AC or PPC neuronal population activity
407 during that trial and calculated the decoding accuracy using five-fold cross validation. Population
408 activity was aligned to turn onset and five seconds of activity leading up to turn onset were used
409 to train the SVM.

410 For comparing the population decoding of stimulus and choice information across
411 performance states, we first separated trials based on the state as identified by the three state
412 GLM-HMM. Due to the higher percentage of state-1 trials in comparison to state 2 and 3 trials,
413 particularly in the behavioral sessions in which imaging was performed, we separated data into
414 two groups for this decoding approach. The first group ('Exclusively State 1') included data

exclusively from state-1 trials and the second group ('All States') included data from state 2 and state 3 trials supplemented with subsampled state-1 trials to ensure a similar amount of trials for comparisons between groups. For each group, within the training dataset (70% of trials), we ensured that cross-validation folds were balanced with a structured distribution of trials from each stimulus and choice combination (left stimulus left choice, right stimulus right choice, left stimulus right choice, right stimulus left choice, Extended Figure 3A). The test dataset (30% of trials) also had a similar distribution of trial conditions and was left out of the fitting procedure. For the stimulus information decoder, neural population activity was aligned to sound onset and for the choice information decoder, neural population activity was aligned to turn onset. All decoders were again built and trained using the sklearn.svm python package. Independent SVMs were trained and tested at each time point, and decoding accuracy was expressed as the proportion of correct classifications across the folds of cross-validation.

GLM encoding models:

Our GLM based encoding models allowed us to model, for each single AC and PPC neuron, the time-dependent effects of various task and behavioral variables on neuronal activity during single trials in a specific recording session. We extend the approaches taken in (Pillow et al., 2008; Runyan et al., 2017; Tseng et al., 2022; Weber & Pillow, 2017) to account for performance state by using separate encoding models for exclusively state-1 trials and another model for trials spanning all states. Again, due to the higher percentage of state-1 trials in comparison to state 2 and 3 trials, particularly in the behavioral sessions in which imaging was performed, we separated data into two groups for this decoding approach. The first group included data exclusively from state-1 trials and the second group included data from state 2 and state 3 trials supplemented with subsampled state-1 trials to ensure a similar amount of trials for comparisons between groups. We used a Bernoulli GLM to weight task variables or task variables + functional coupling variables (principal components of population activity) in predicting a single neuron's binary activity.

Task-related model predictors

A total of 419 task-related predictors (420 when including a constant predictor corresponding to the average activation probability of each individual neuron) were used in all encoding models. The behavioral variables included the running velocity on the pitch and roll axes of the spherical treadmill, x and y position, onset times and locations of sound stimuli, view angle of the mouse in the VR maze, turn direction, and reward and error signal delivery times. A detailed description of the selection, construction, and normalization parameters of task-related predictors using various sets of basis-functions can be found in Runyan et al., 2017.

Functional coupling model predictors

We developed encoding models with functional coupling predictors to compare the dependence of each neuron's activity on task-related information correlates and the activity of the other neurons in the population. Previous work has used the relative spike rate of each other neuron excluding the neuron being fitted and convolved the spike rate with boxcar functions, however we took a dimensionality reduction approach to reduce the number of total coupling predictors. We first excluded the neuron being fit by the encoding model and performed principal component analysis (PCA) along ~1 second time bins on the matrix of spiking activity of all other neurons in the local population for that imaging session using the sklearn.decomposition.pca python function. We then took the first five principal components (PCs), which accounted for ~65-70% of the overall variance in the population activity. We then maximum-normalized and z-scored the PCs and convolved the PCs using two evenly spaced Gaussian basis functions extending ~120ms second forwards and backwards in time which yielded 10 total 'functional coupling' predictors.

GLM fitting procedure:

All task-related information and functional coupling predictors were maximum-normalized, and z-scored before fitting each encoding model. We fitted the GLMs to each single neuron's activity using the GLM_tensorflow_2 python package. We used an elastic net regularized GLM

467 which interpolates between L_1 and L_2 regularization penalties based on the interpolation
468 parameter α. We used α = .95 to allow for a relatively small number of predictors to be selected
469 by the model. Within the training dataset (70% of trials), cross-validation folds were balanced with
470 a structured distribution of trials from each stimulus and choice combination (Extended Figure
471 3A). The test dataset (30% of trials), also containing a similar distribution of trial conditions, was
472 left out of the fitting procedure entirely, and was used only for testing the model performance.
473 Each model was thus fitted and tested on entirely separate data, removing over-fitting concerns.
474 This train and test procedure was repeated ten times, with random subsamples of the data
475 included in train and test segments.

476 *GLM model performance:*

477 Model performance was quantified by computing the fraction of explained deviance of the
478 fitted model by comparing the deviance of the fitted model with the deviance of null model of each
479 neuron's activity that used a single constant parameter. This null model lacked time-varying task
480 predictors or functional coupling predictors. Thus, the fraction of explained deviance was
481 calculated as ((null deviance – fitted model deviance) / null deviance). All deviance calculation
482 were calculated on the test dataset for all folds of the encoding models for each neuron.

483 *Pairwise noise correlations:*

484 Pairwise noise correlations were calculated based on trial-to-trial fluctuations around
485 mean sound-evoked responses. PPC neuronal activity for each trial is aligned to turn onset and
486 AC neuronal activity for each trial is aligned to first sound onset. We then calculated the mean
487 sensory-evoked activity for each neuron for each of the eight possible sound locations and binned
488 the activity of each neuron by 1s over the course of the sound trial. For each neuron, we
489 subtracted the corresponding mean sensory evoked responses from single trial activity, and then
490 concatenated these mean-subtracted trial responses. For each pair of neurons, we computed the
491 Pearson correlation coefficient between these binned, mean-subtracted activity timeseries using
492 the np.corrcoef python function.

References

Akrami, A., Kopec, C. D., Diamond, M. E., & Brody, C. D. (2018). Posterior parietal cortex represents sensory history and mediates its effects on behaviour. *Nature*, *554*(7692), 368–372. https://doi.org/10.1038/nature25510

Aponte, D. A., Handy, G., Kline, A. M., Tsukano, H., Doiron, B., & Kato, H. K. (2021). Recurrent network dynamics shape direction selectivity in primary auditory cortex. *Nature Communications*, *12*(1). https://doi.org/10.1038/s41467-020-20590-6

Aronov, D., & Tank, D. W. (2014). Engagement of Neural Circuits Underlying 2D Spatial Navigation in a Rodent Virtual Reality System. *Neuron*, *84*(2), 442–456. https://doi.org/10.1016/j.neuron.2014.08.042

Aschauer, D. F., Eppler, J. B., Ewig, L., Chambers, A. R., Pokorny, C., Kaschube, M., & Rumpel, S. (2022). Learning-induced biases in the ongoing dynamics of sensory representations predict stimulus generalization. *Cell Reports*, *38*(6). https://doi.org/10.1016/j.celrep.2022.110340

Ashwood, Z. C., Roy, N. A., Stone, I. R., Urai, A. E., Churchland, A. K., Pouget, A., & Pillow, J. W. (2022). Mice alternate between discrete strategies during perceptual decision-making. *Nature Neuroscience*, *25*(2), 201–212. https://doi.org/10.1038/s41593-021-01007-z

Bigelow, J., Morrill, R. J., Dekloe, J., & Hasenstaub, A. R. (2019). Movement and VIP interneuron activation differentially modulate encoding in mouse auditory cortex. *ENeuro*, *6*(5). https://doi.org/10.1523/ENEURO.0164-19.2019

Bolkan, S. S., Stone, I. R., Pinto, L., Ashwood, Z. C., Iravedra Garcia, J. M., Herman, A. L., Singh, P., Bandi, A., Cox, J., Zimmerman, C. A., Cho, J. R., Engelhard, B., Pillow, J. W., & Witten, I. B. (2022). Opponent control of behavior by dorsomedial striatal pathways depends on task demands and internal state. *Nature Neuroscience*, *25*(3), 345–357. https://doi.org/10.1038/s41593-022-01021-9

Downer, J. D., Bigelow, J., Runfeldt, M. J., & Malone, B. J. (2021). Temporally precise population coding of dynamic sounds by auditory cortex. *Journal of Neurophysiology*, *126*(1), 148–169. https://doi.org/10.1152/jn.00709.2020

Driscoll, L. N., Pettit, N. L., Minderer, M., Chettih, S. N., & Harvey, C. D. (2017). Dynamic Reorganization of Neuronal Activity Patterns in Parietal Cortex. *Cell*, *170*(5), 986-999.e16. https://doi.org/10.1016/j.cell.2017.07.021

Flavell, S. W., Gogolla, N., Lovett-Barron, M., & Zelikowsky, M. (2022). The emergence and influence of internal states. In *Neuron* (Vol. 110, Issue 16, pp. 2545–2570). Cell Press. https://doi.org/10.1016/j.neuron.2022.04.030

Fritz, J., Shamma, S., Elhilali, M., & Klein, D. (2003). Rapid task-related plasticity of spectrotemporal receptive fields in primary auditory cortex. *Nature Neuroscience*, *6*(11), 1216–1223. https://doi.org/10.1038/nn1141

Goard, M. J., Pho, G. N., Woodson, J., & Sur, M. (n.d.). *Distinct roles of visual, parietal, and frontal motor cortices in memory-guided sensorimotor decisions*. https://doi.org/10.7554/eLife.13764.001

Guo, L., Ponvert, N. D., & Jaramillo, S. (2017). The role of sensory cortex in behavioral flexibility. In *Neuroscience* (Vol. 345, pp. 3–11). Elsevier Ltd. https://doi.org/10.1016/j.neuroscience.2016.03.067

Harris, K. D., & Thiele, A. (2011). Cortical state and attention. In *Nature Reviews Neuroscience* (Vol. 12, Issue 9, pp. 509–523). https://doi.org/10.1038/nrn3084

Harvey, C. D., Coen, P., & Tank, D. W. (2012). Choice-specific sequences in parietal cortex during a virtual-navigation decision task. *Nature*, *484*(7392), 62–68. https://doi.org/10.1038/nature10918

Heller, C. R., Hamersky, G. R., & David, S. V. (2023). *Task-specific invariant representation in auditory cortex*. eLife. https://doi.org/10.7554/eLife.89936.1

Hulsey, D., Zumwalt, K., Mazzucato, L., McCormick, D. A., & Jaramillo, S. (2024). Decision-making dynamics are predicted by arousal and uninstructed movements. *Cell Reports*, *43*(2), 113709. https://doi.org/10.1016/j.celrep.2024.113709

Khoury, C. F., Fala, N. G., & Runyan, C. A. (2023). Arousal and Locomotion Differently Modulate Activity of Somatostatin Neurons across Cortex. *ENeuro*, *10*(5). https://doi.org/10.1523/ENEURO.0136-23.2023

Kuchibhotla, K. V., Gill, J. V., Lindsay, G. W., Papadoyannis, E. S., Field, R. E., Sten, T. A. H., Miller, K. D., & Froemke, R. C. (2017). Parallel processing by cortical inhibition enables context-dependent behavior. *Nature Neuroscience*, *20*(1), 62–71. https://doi.org/10.1038/nn.4436

Lin, P. A., Asinof, S. K., Edwards, N. J., & Isaacson, J. S. (2019). Arousal regulates frequency tuning in primary auditory cortex. *Proceedings of the National Academy of Sciences of the United States of America*, *116*(50), 25304–25310. https://doi.org/10.1073/pnas.1911383116

Livneh, Y., & Andermann, M. L. (2021). Cellular activity in insular cortex across seconds to hours: Sensations and predictions of bodily states. In *Neuron* (Vol. 109, Issue 22, pp. 3576–3593). Cell Press. https://doi.org/10.1016/j.neuron.2021.08.036

Lyamzin, D., & Benucci, A. (2019). The mouse posterior parietal cortex: Anatomy and functions. In *Neuroscience Research* (Vol. 140, pp. 14–22). Elsevier Ireland Ltd. https://doi.org/10.1016/j.neures.2018.10.008

McGinley, M. J., David, S. V., & McCormick, D. A. (2015). Cortical Membrane Potential Signature of Optimal States for Sensory Signal Detection. *Neuron*, *87*(1), 179–192. https://doi.org/10.1016/j.neuron.2015.05.038

Minderer, M., Brown, K. D., & Harvey, C. D. (2019). The Spatial Structure of Neural Encoding in Mouse Posterior Cortex during Navigation. *Neuron*, *102*(1), 232-248.e11. https://doi.org/10.1016/j.neuron.2019.01.029

Mohan, K., Zhu, O., & Freedman, D. J. (2021). Interaction between neuronal encoding and population dynamics during categorization task switching in parietal cortex. *Neuron*, *109*(4), 700-712.e4. https://doi.org/10.1016/j.neuron.2020.11.022

Musall, S., Kaufman, M. T., Juavinett, A. L., Gluf, S., & Churchland, A. K. (2019). Single-trial neural dynamics are dominated by richly varied movements. *Nature Neuroscience*, *22*(10), 1677–1686. https://doi.org/10.1038/s41593-019-0502-4

Nelson, A., & Mooney, R. (2016). The Basal Forebrain and Motor Cortex Provide Convergent yet Distinct Movement-Related Inputs to the Auditory Cortex. *Neuron*, *90*(3), 635–648. https://doi.org/10.1016/j.neuron.2016.03.031

Pho, G. N., Goard, M. J., Woodson, J., Crawford, B., & Sur, M. (2018). Task-dependent representations of stimulus and choice in mouse parietal cortex. *Nature Communications*, *9*(1). https://doi.org/10.1038/s41467-018-05012-y

Pillow, J. W., Shlens, J., Paninski, L., Sher, A., Litke, A. M., Chichilnisky, E. J., & Simoncelli, E. P. (2008). Spatio-temporal correlations and visual signalling in a complete neuronal population. *Nature*, *454*(7207), 995–999. https://doi.org/10.1038/nature07140

Runyan, C. A., Piasini, E., Panzeri, S., & Harvey, C. D. (2017). Distinct timescales of population coding across cortex. *Nature*, *548*(7665), 92–96. https://doi.org/10.1038/nature23020

Schneider, D. M., Nelson, A., & Mooney, R. (2014). A synaptic and circuit basis for corollary discharge in the auditory cortex. *Nature*, *513*(7517), 189–194. https://doi.org/10.1038/nature13724

Schneider, D. M., Sundararajan, J., & Mooney, R. (2018). A cortical filter that learns to suppress the acoustic consequences of movement. *Nature*, *561*(7723), 391–395. https://doi.org/10.1038/s41586-018-0520-5

Song, Y. H., Kim, J. H., Jeong, H. W., Choi, I., Jeong, D., Kim, K., & Lee, S. H. (2017). A Neural Circuit for Auditory Dominance over Visual Perception. *Neuron*, *93*(4), 940-954.e6. https://doi.org/10.1016/j.neuron.2017.01.006

Steinmetz, N. A., Zatka-Haas, P., Carandini, M., & Harris, K. D. (2019). Distributed coding of choice, action and engagement across the mouse brain. *Nature*, *576*(7786), 266–273. https://doi.org/10.1038/s41586-019-1787-x

Tseng, S.-Y., Chettih, S. N., Arlt, C., Barroso-Luque, R., & Harvey, C. D. (2022). Shared and specialized coding across posterior cortical areas for dynamic navigation decisions. *Neuron*. https://doi.org/10.1016/j.neuron.2022.05.012

Valente, M., Pica, G., Bondanelli, G., Moroni, M., Runyan, C. A., Morcos, A. S., Harvey, C. D., & Panzeri, S. (2021). Correlations enhance the behavioral readout of neural population activity in association cortex. *Nature Neuroscience*, *24*(7), 975–986. https://doi.org/10.1038/s41593-021-00845-1

Weber, A. I., & Pillow, J. W. (2017). Capturing the dynamical repertoire of single neurons with generalized linear models. In *Neural Computation* (Vol. 29, Issue 12, pp. 3260–3289). MIT Press Journals. https://doi.org/10.1162/NECO_a_01021

Yin, C., Melin, M. D., Rojas-Bowe, G., Sun, X. R., Gluf, S., Couto, J., Kostiuk, A., Musall, S., & Churchland, A. K. (2023). Engaged decision-makers align spontaneous movements to stereotyped task demands. *BioRxiv : The Preprint Server for Biology*. https://doi.org/10.1101/2023.06.26.546404

Zhong, L., Zhang, Y., Duan, C. A., Deng, J., Pan, J., & Xu, N. long. (2019). Causal contributions of parietal cortex to perceptual decision-making during stimulus categorization. *Nature Neuroscience*, *22*(6), 963–973. https://doi.org/10.1038/s41593-019-0383-6

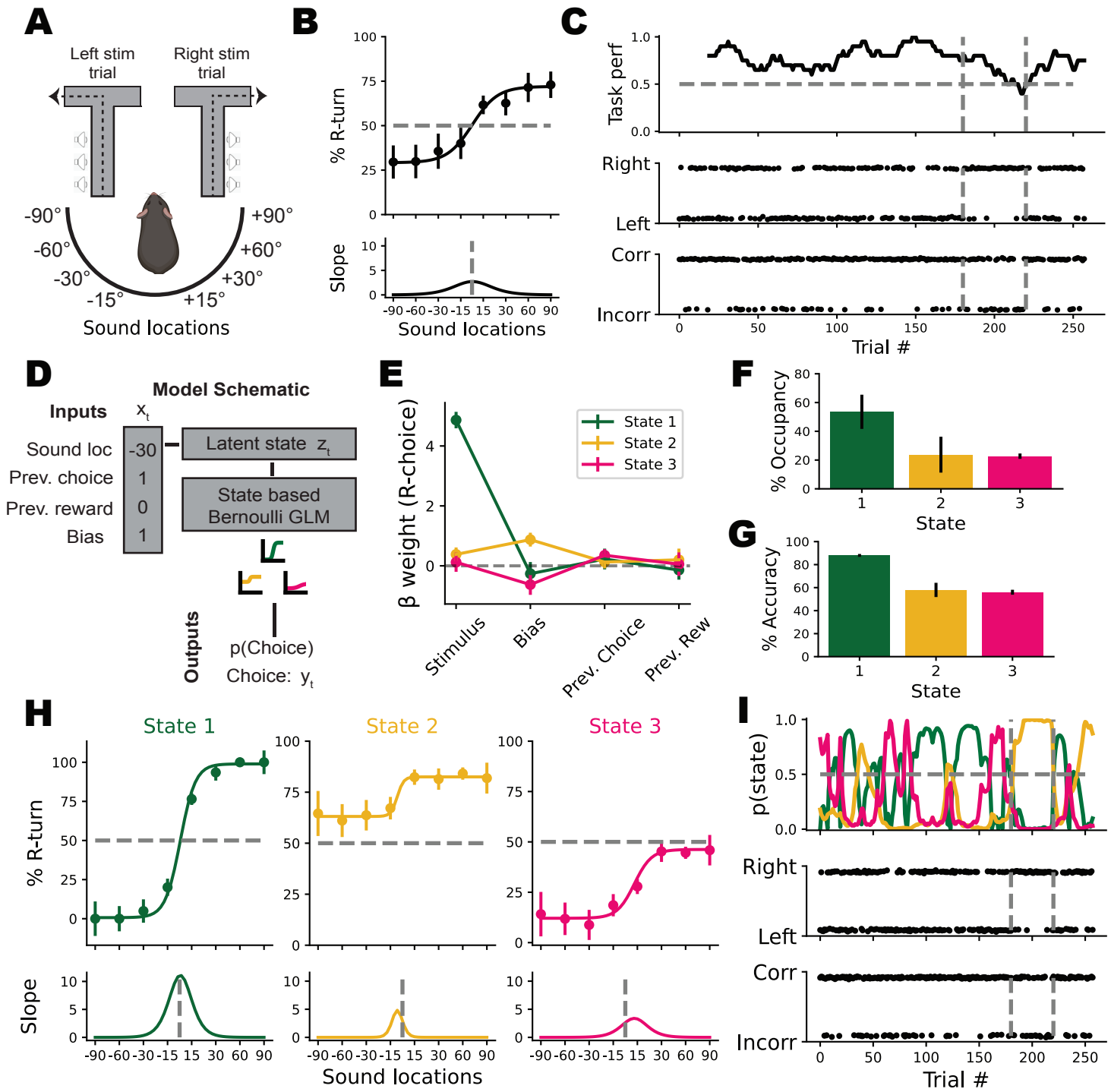

Figure 1. Mice switch between different performance states during auditory decision-making. (A) Mice were trained to report the location of a sound stimulus by turning in the direction of the sound in a virtual-reality T-maze. **(B)** Mice learned to categorize sound locations and performed the task (n=5 mice, mean ± s.e.m) as evidenced by the psychometric curve for the probability of a right-ward choice given a sound stimulus for a specific location **(C, top)** Performance of an example mouse in one behavioral session presented as a 20-trial moving window of correct choices. Vertical dashed lines indicate a period of trials where the mouse's performance dropped below chance level. **(C, middle)** Left or right choice identity for each trial. **(C, bottom)** Correct or incorrect identity for each trial. **(D)** Three-state GLM-HMM model with four input variables and three different GLMs corresponding to different decision-making strategies. **(E)** Inferred GLM weights for the three-state GLM-HMM. State 1 has a high weight for stimulus information, and states 2 and 3 have high and opposing weights for bias (n=5 mice, mean ± s.e.m). **(F)** Fractional occupancies for each state across all behavioral trials used in fitting the global three state GLM-HMM. State 1 is the most occupied (n=17,602 trials, mean ± s.e.m). **(G)** Task accuracy across each GLM-HMM state (n=17,602 trials, mean ± s.e.m). **(H)** Per-state psychometric curves for the probability of a right-ward choice given a sound stimulus for a specific location. The different psychometrics across the three states highlight differences in decision-making strategy and performance (n=17,602 trials, mean ± s.e.m). **(I, top)** Posterior state probability for the example session shown in C. The three-state model successfully identifies the period of poor task performance and classifies the animal's behavior as being in state 2, which is characterized by rightward bias.

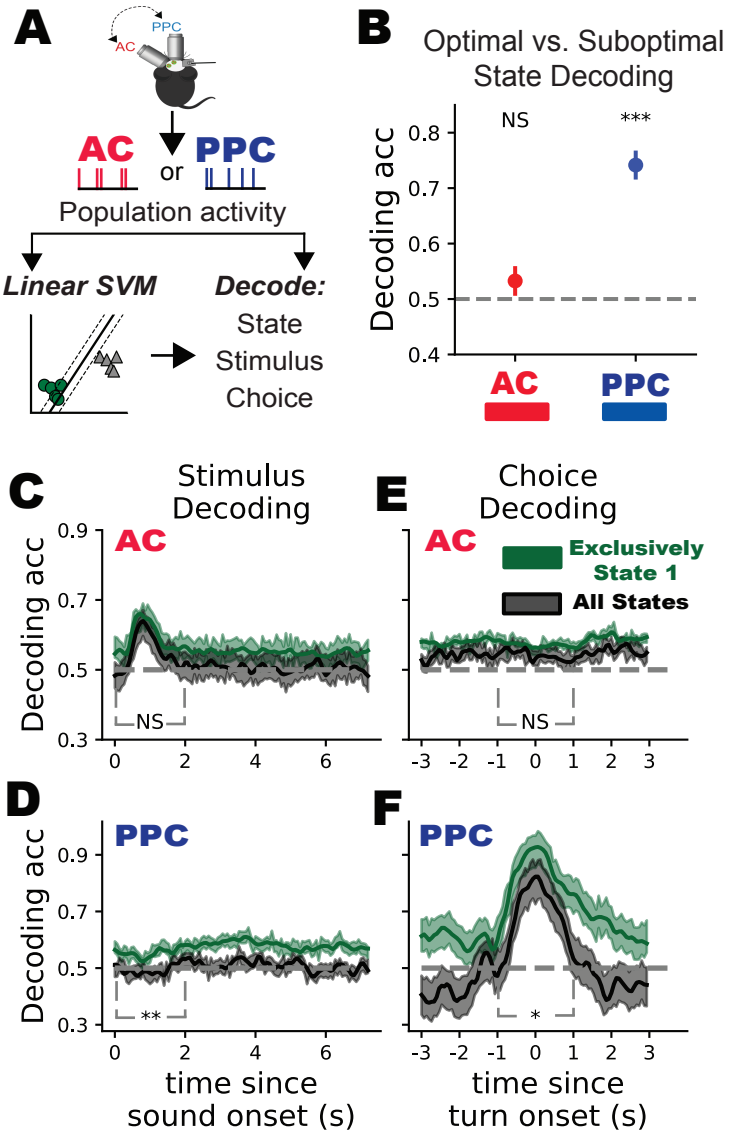

Figure 2. Performance states differently impact information coding in sensory and association cortex population activity. (A) Schematic of using a linear SVM to decode state, stimulus, and choice information from AC and PPC population activity. **(B)** SVM decoding accuracy of the classification of a trial as occuring during the optimal or suboptimal state from PPC or AC population activity during that trial (n=6 recording sessions, mean ± s.e.m, AC: p= 0.67, PPC: p= 5.9 x 10-7, Wilcoxon signed rank test). **(C)** SVM decoding accuracy of stimulus information from AC population activity at each time point in the trial. Green indicates decoding from exclusively state 1 trial, and black indicates decoding from trials spanning all three states (n=6 recording sessions, mean ± s.e.m, p= .82, Wilcoxon signed rank test). **(D)** SVM decoding accuracy of stimulus information from PPC population activity (n=6 recording sessions, mean ± s.e.m, p= .44, Wilcoxon signed rank test). **(E)** SVM decoding accuracy of choice information from AC population activity (n=6 recording sessions, mean ± s.e.m, p= .004, Wilcoxon signed rank test). **(F)** SVM decoding accuracy of stimulus information from PPC population activity (n=6 recording sessions, mean ± s.e.m, p= .038, Wilcoxon signed rank test).

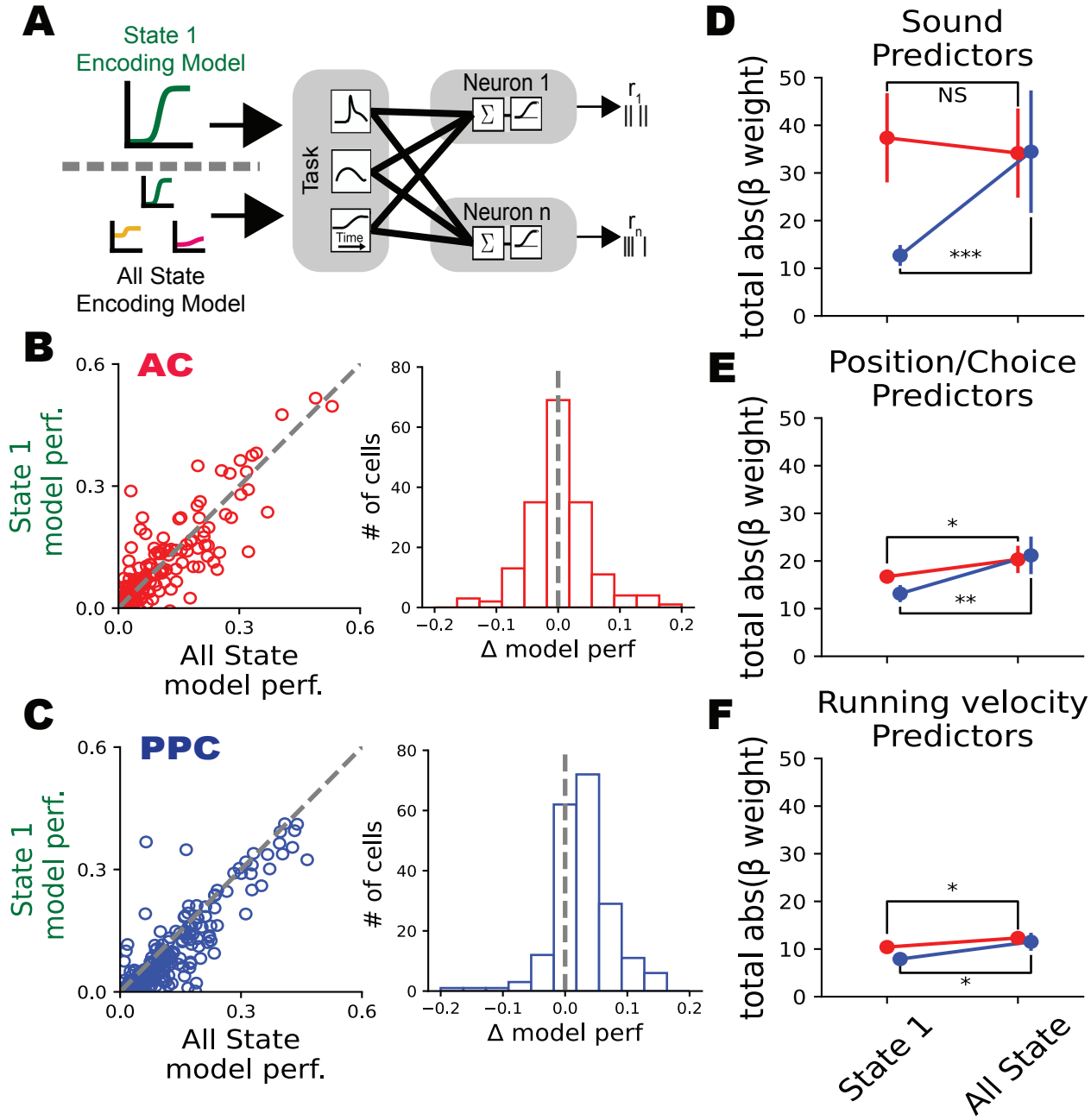

Figure 3. Behavioral variables better predict PPC but not AC neuronal activity during suboptimal performance states. **(A)** Model schematic for two GLM-based encoding models. The state 1 encoding model was trained to predict neuronal activity given task information from exclusively state-1 trials. The all-state model was trained to predict neuronal activity given task information from trials spanning all three states. **(B, C - left)** Prediction performance of the state 1 model and all-state model for all AC and PPC neurons. **(B, C – right)** Histograms showing the distribution of the difference in prediction performance of the two model types across all AC and PPC neurons (n=171 AC neurons, n=203 PPC neurons). **(D)** Fitted model weights for variables related to sound location between the two model types averaged across AC (red) and PPC (blue) neurons. (n=171 AC neurons, n=203 PPC neurons, mean ± s.e.m, AC comparison: p=.384, PPC comparison: p=.001, Mann-Whitney U-test). **(E)** Fitted model weights for variables related to position and choice between the two model types averaged across AC and PPC neurons. (n=171 AC neurons, n=203 PPC neurons, mean ± s.e.m, AC comparison: p=.014, PPC comparison: p=.005, Mann-Whitney U-test). **(F)** Fitted model weights for variables related to running between the two model types averaged across AC and PPC neurons. (n=171 AC neurons, n=203 PPC neurons, mean ± s.e.m, AC comparison: p=.011, PPC comparison: p=.037, Mann-Whitney U-test).

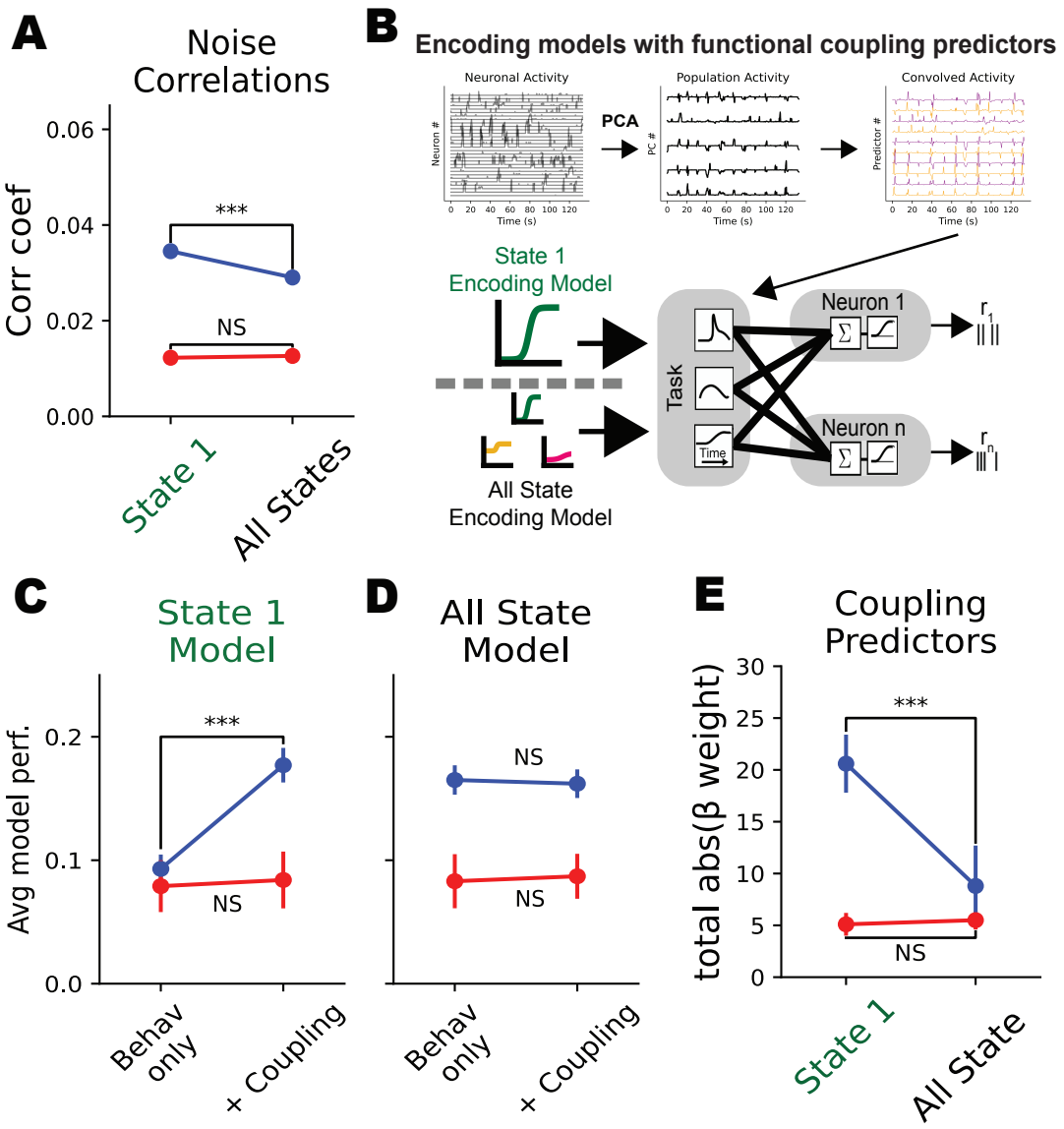

Figure 4. Functional coupling drives PPC neuronal activity only during optimal performance states. (A) Comparison of the pairwise noise correlations between all AC (red) or PPC (blue) neurons from exclusively state 1 trials or trials spanning all three states (AC: p=.096, PPC: p=2.4 x 10-9, Mann-Whitney U-test). **(B)** Model schematic for two GLM-based encoding models with population activity functional coupling predictors **(C)** Comparison of average model performance between the state-1 encoding model with only behavioral task information as predictors of neuronal activity (n=171 AC neurons, n=203 PPC neurons, mean ± s.e.m, AC: p=.438, PPC: p=6.2 x 10-5, Mann-Whitney U-test) and the all-state encoding model with both behavioral task information and functional coupling as predictors of neuronal activity. (n=171 AC neurons, n=203 PPC neurons, mean ± s.e.m, AC: p=.106, PPC: p=.588, Mann-Whitney U-test). **(D)** Comparison of average model performance between the state-1 encoding model with only behavioral task information as predictors of neuronal activity and the state-1 encoding model with both behavioral task information and functional coupling as predictors of neuronal activity. **(E)** Fitted model weights for coupling predictors between the two model types averaged across AC and PPC neurons (n=171 AC neurons, n=203 PPC neurons, mean ± s.e.m, AC comparison: p=.278, PPC comparison: p=1.0 x 10-4, Mann-Whitney U-test).

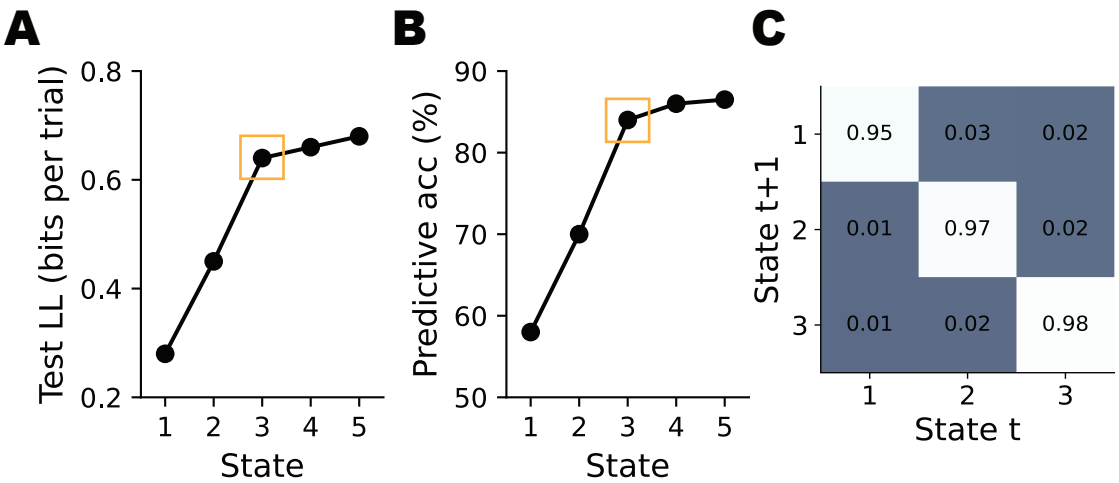

Extended Figure 1. GLM-HMM cross validation. (A) Model comparison of GLM-HMMs with different number of latent states using test log likelihood (in bits per trial) from five-fold cross validation. **(B)** Prediction accuracy (percentage of held out test trials the model correctly predicted the mouse's choice) of GLM-HMMs with different number of latent states. **(C)** Inferred transition probability matrix for global three state GLM-HMM.

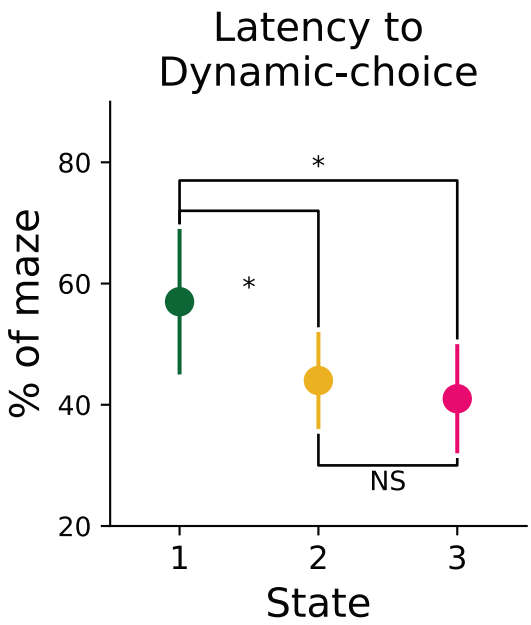

Extended Figure 2. Choice formation is slower in the optimal performance state. We quantified how well running trajectories in a single trial predicted the mouse's upcoming choice on that trial using a long short-term memory (LSTM) recurrent neural network (Tseng et al., 2022). For each time point in the trial the LSTM used running variables such as X/Y position, X/Y velocity, and view angle in the maze from all previous time points to estimate the probability that the mouse turned left or right. We then measured the latency to dynamic choice as the time point where the model's prediction exceeded a threshold of 0.9 for left choice trials and 0.1 for right choice trials. We examined the latency to dynamic choice for all three GLM-HMM latent states across all behavioral sessions and found that the latency to dynamic choice, was significantly higher in the optimal state (state 1) than in the two suboptimal states (state 1 vs state 2, p=0.024. state 2 vs state 2, p=0.011. state 2 vs state 3, p=.680. Mann-Whitney U-test).

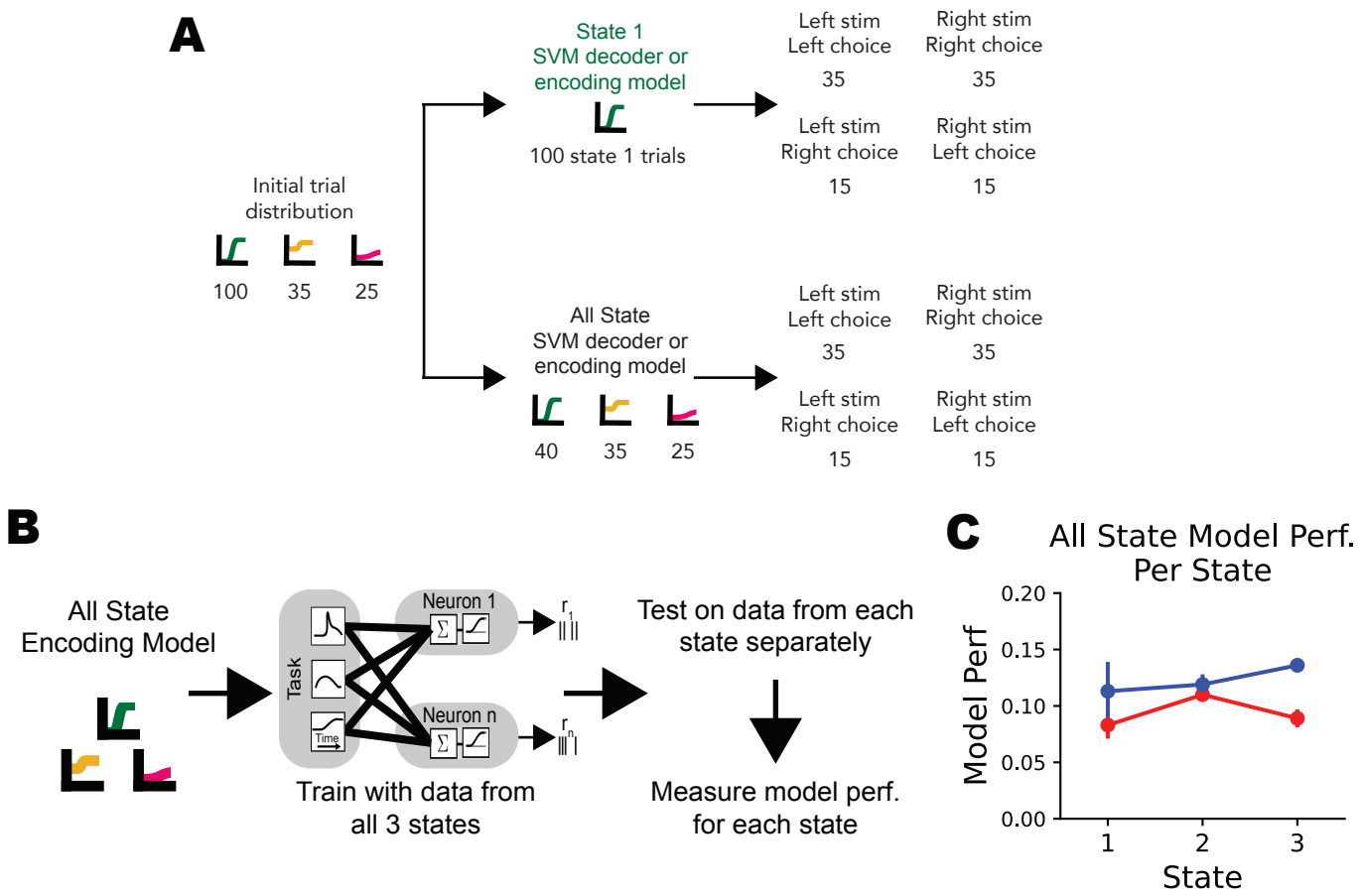

Extended Figure 3. All state encoding model performance across trials from each GLM-HMM state. (A) Schematic of trial type distribution for each model (SVM decoders + GLM encoding models). **(B)** Model schematic for the all-state encoding model trained on neuronal activity given task information from trials spanning all three states and then tested on trials from each of the three states separately to measure the model performance for each state. **(C)** Model performance for each state for AC neurons (red) and PPC neurons (blue) show consistent performance across all states.

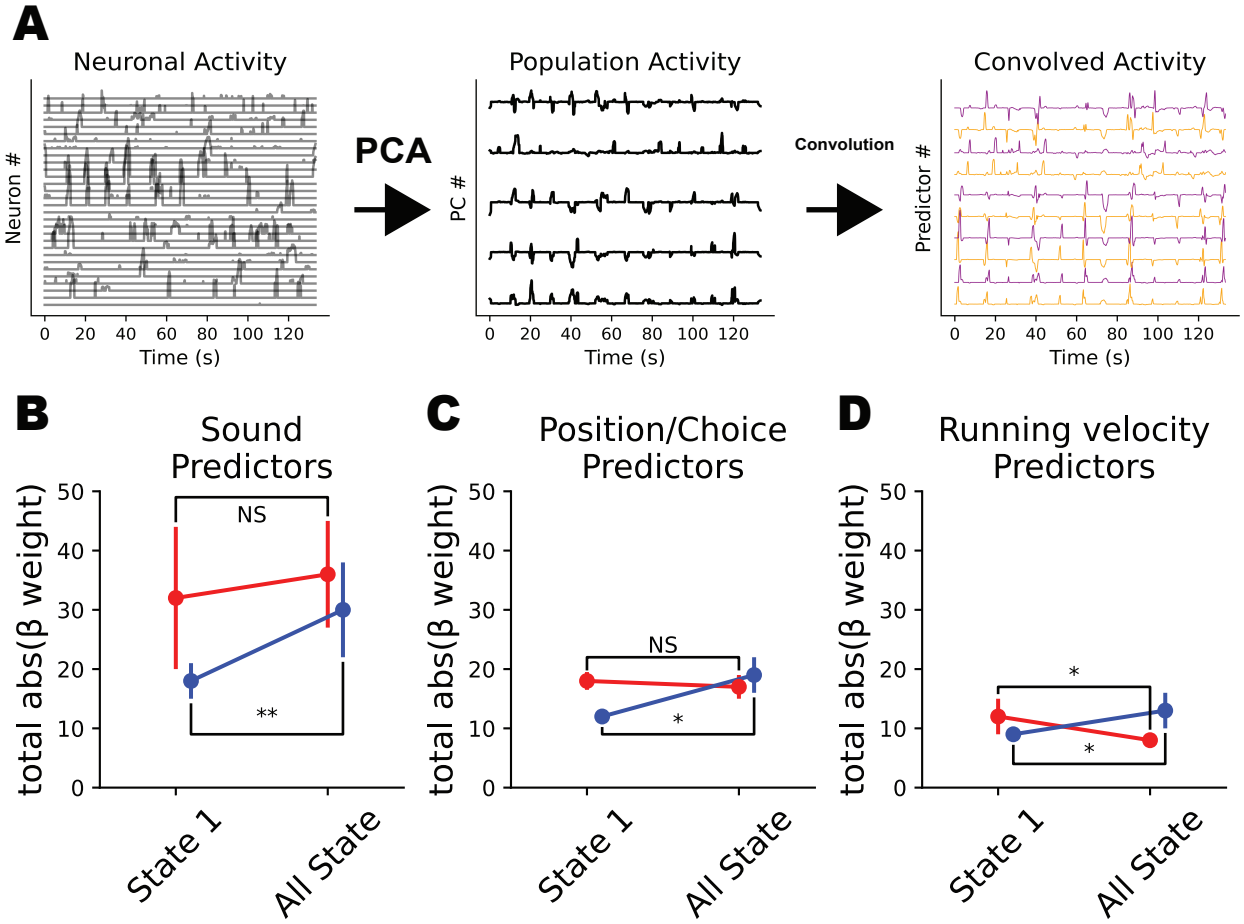

Extended Figure 4. The all-state encoding model with coupling has model weights consistent to the all-state encoding model without coupling. (A) Schematic of the PCA based population activity functional coupling predictors used in the encoding models presented in figure 4. **(B)** Fitted model weights for variables related to sound location between the two model types averaged across AC (red) and PPC (blue) neurons. (AC comparison: p=.602, PPC comparison: p=.018, Mann-Whitney U-test). **(C)** Fitted model weights for variables related to position and choice between the two model types averaged across AC and PPC neurons. (AC comparison: p=.088, PPC comparison: p=.030, Mann-Whitney U-test). **(D)** Fitted model weights for variables related to running between the two model types averaged across AC and PPC neurons. (AC comparison: p=.025, PPC comparison: p=.022, Mann-Whitney U-test).